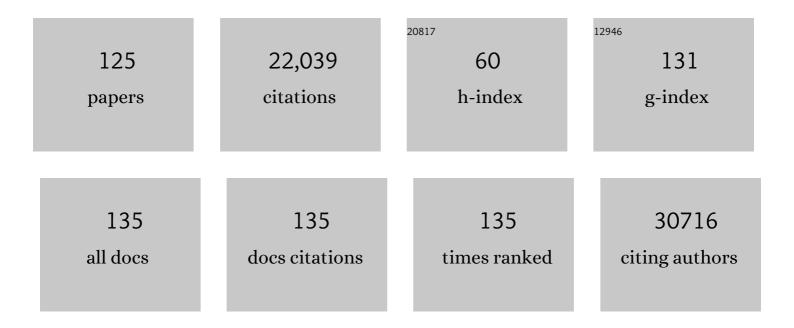
Hyeon S Shin

List of Publications by Year in descending order

Source: https://exaly.com/author-pdf/7418049/publications.pdf Version: 2024-02-01



#	Article	IF	CITATIONS
1	High-yield production of mono- or few-layer transition metal dichalcogenide nanosheets by an electrochemical lithium ion intercalation-based exfoliation method. Nature Protocols, 2022, 17, 358-377.	12.0	100
2	Epitaxial single-crystal hexagonal boron nitride multilayers on Ni (111). Nature, 2022, 606, 88-93.	27.8	97
3	Large-Area Hexagonal Boron Nitride Layers by Chemical Vapor Deposition: Growth and Applications for Substrates, Encapsulation, and Membranes. Accounts of Materials Research, 2022, 3, 748-760.	11.7	13
4	Synthesis of 1T WSe ₂ on an Oxygen-Containing Substrate Using a Single Precursor. ACS Nano, 2022, 16, 11059-11065.	14.6	9
5	Synthesis of metallic mixed 3R and 2H Nb _{1+x} S ₂ nanoflakes by chemical vapor deposition. Faraday Discussions, 2021, 227, 332-340.	3.2	2
6	Vertically oriented MoS ₂ /WS ₂ heterostructures on reduced graphene oxide sheets as electrocatalysts for hydrogen evolution reaction. Materials Chemistry Frontiers, 2021, 5, 3396-3403.	5.9	20
7	Reply to: On the measured dielectric constant of amorphous boron nitride. Nature, 2021, 590, E8-E10.	27.8	1
8	Toward growth of wafer-scale single-crystal hexagonal boron nitride sheets. Nano Express, 2021, 2, 031004.	2.4	3
9	Interlayer electron modulation in van der Waals heterostructures assembled by stacking monolayer MoS ₂ onto monolayer graphene with different electron transfer ability. Nanoscale, 2021, 13, 15464-15470.	5.6	6
10	Modulation of Cu and Rh single-atoms and nanoparticles for high-performance hydrogen evolution activity in acidic media. Journal of Materials Chemistry A, 2021, 9, 10326-10334.	10.3	70
11	Strong exciton-photon coupling in large area MoSe2 and WSe2 heterostructures fabricated from two-dimensional materials grown by chemical vapor deposition. 2D Materials, 2021, 8, 011002.	4.4	10
12	Proton conductivity of a hexagonal boron nitride membrane and its energy applications. Journal of Materials Chemistry A, 2020, 8, 2898-2912.	10.3	27
13	Blue emission at atomically sharp 1D heterojunctions between graphene and h-BN. Nature Communications, 2020, 11, 5359.	12.8	23
14	Radio-frequency-transmitting hexagonal boron nitride-based anti- and de-icing heating system. Nanoscale, 2020, 12, 21895-21900.	5.6	7
15	Large area chemical vapour deposition grown transition metal dichalcogenide monolayers automatically characterized through photoluminescence imaging. Npj 2D Materials and Applications, 2020, 4, .	7.9	20
16	Effect of Pt Crystal Surface on Hydrogenation of Monolayer h-BN and Its Conversion to Graphene. Chemistry of Materials, 2020, 32, 4584-4590.	6.7	9
17	Ultralow-dielectric-constant amorphous boron nitride. Nature, 2020, 582, 511-514.	27.8	173
18	Recent Developments in Synthesis and Photocatalytic Applications of Carbon Dots. Catalysts, 2020, 10, 320.	3.5	54

#	Article	IF	CITATIONS
19	General Colloidal Synthesis of Transition-Metal Disulfide Nanomaterials as Electrocatalysts for Hydrogen Evolution Reaction. ACS Applied Materials & Interfaces, 2020, 12, 13148-13155.	8.0	25
20	Spatially controlled lateral heterostructures of graphene and transition metal dichalcogenides toward atomically thin and multi-functional electronics. Nanoscale, 2020, 12, 5286-5292.	5.6	8
21	Direct Epitaxial Synthesis of Selective Two-Dimensional Lateral Heterostructures. ACS Nano, 2019, 13, 13047-13055.	14.6	52
22	Quantum Efficiency Enhancement of Bialkali Photocathodes by an Atomically Thin Layer on Substrates. Physica Status Solidi (A) Applications and Materials Science, 2019, 216, 1900501.	1.8	6
23	Ultrahigh-current-density niobium disulfide catalysts for hydrogen evolution. Nature Materials, 2019, 18, 1309-1314.	27.5	280
24	Chalcogenide solution-mediated activation protocol for scalable and ultrafast synthesis of single-crystalline 1-D copper sulfide for supercapacitors. Journal of Materials Chemistry A, 2019, 7, 2529-2535.	10.3	19
25	Highâ€Performance Hydrogen Evolution by Ru Single Atoms and Nitridedâ€Ru Nanoparticles Implanted on Nâ€Đoped Graphitic Sheet. Advanced Energy Materials, 2019, 9, 1900931.	19.5	224
26	Radio Frequency Transmission: Improving Radio Frequency Transmission Properties of Graphene via Carrier Concentration Control toward High Frequency Transmission Line Applications (Adv. Funct.) Tj ETQq0 0 0	rg B 4.¢Ove	rlook 10 Tf 50
27	Resonantly hybridized excitons in moiré superlattices in van der Waals heterostructures. Nature, 2019, 567, 81-86.	27.8	621
28	Dendritic Multipods: Sphere-to-Multipod Transmorphic Change of Nanoconfined Pt Electrocatalyst during Oxygen Reduction Reaction (Small 2/2019). Small, 2019, 15, 1970013.	10.0	0
29	Improving Radio Frequency Transmission Properties of Graphene via Carrier Concentration Control toward High Frequency Transmission Line Applications. Advanced Functional Materials, 2019, 29, 1808057.	14.9	6
30	Surface functionalization-induced photoresponse characteristics of monolayer MoS ₂ for fast flexible photodetectors. Nanoscale, 2019, 11, 4726-4734.	5.6	44
31	Layered material platform for surface plasmon resonance biosensing. Scientific Reports, 2019, 9, 20286.	3.3	55
32	Planar and van der Waals heterostructures for vertical tunnelling single electron transistors. Nature Communications, 2019, 10, 230.	12.8	43
33	Rapid synthesis of graphene by chemical vapor deposition using liquefied petroleum gas as precursor. Carbon, 2019, 145, 462-469.	10.3	23
34	Sphereâ€ŧoâ€Multipod Transmorphic Change of Nanoconfined Pt Electrocatalyst during Oxygen Reduction Reaction. Small, 2019, 15, e1802228.	10.0	12
35	Efficient Hydrogen Evolution Reaction Catalysis in Alkaline Media by Allâ€inâ€One MoS ₂ with Multifunctional Active Sites. Advanced Materials, 2018, 30, e1707105.	21.0	321
36	Low-dimensional catalysts for hydrogen evolution and CO2 reduction. Nature Reviews Chemistry, 2018, 2, .	30.2	631

#	Article	IF	CITATIONS
37	Electrochemical and electrocatalytic reaction characteristics of boron-incorporated graphene <i>via</i> Âa simple spin-on dopant process. Journal of Materials Chemistry A, 2018, 6, 7351-7356.	10.3	23
38	AA′-Stacked Trilayer Hexagonal Boron Nitride Membrane for Proton Exchange Membrane Fuel Cells. ACS Nano, 2018, 12, 10764-10771.	14.6	55
39	Nafion-Mediated Liquid-Phase Exfoliation of Transition Metal Dichalcogenides and Direct Application in Hydrogen Evolution Reaction. Chemistry of Materials, 2018, 30, 4658-4666.	6.7	30
40	Multicomponent electrocatalyst with ultralow Pt loading and high hydrogen evolution activity. Nature Energy, 2018, 3, 773-782.	39.5	542
41	Chemical Vapor-Deposited Hexagonal Boron Nitride as a Scalable Template for High-Performance Organic Field-Effect Transistors. Chemistry of Materials, 2017, 29, 2341-2347.	6.7	52
42	Hierarchically assembled tubular shell-core-shell heterostructure of hybrid transition metal chalcogenides for high-performance supercapacitors with ultrahigh cyclability. Nano Energy, 2017, 37, 15-23.	16.0	72
43	Study of Cooling Rate on the Growth of Graphene via Chemical Vapor Deposition. Chemistry of Materials, 2017, 29, 4202-4208.	6.7	24
44	2D materials-based photoelectrochemical cells: Combination of transition metal dichalcogenides and reduced graphene oxide for efficient charge transfer. FlatChem, 2017, 4, 54-60.	5.6	18
45	Molecular Beam Epitaxy of Highly Crystalline Monolayer Molybdenum Disulfide on Hexagonal Boron Nitride. Journal of the American Chemical Society, 2017, 139, 9392-9400.	13.7	167
46	Evidence of Local Commensurate State with Lattice Match of Graphene on Hexagonal Boron Nitride. ACS Nano, 2017, 11, 7084-7090.	14.6	31
47	Monolayer optical memory cells based on artificial trap-mediated charge storage and release. Nature Communications, 2017, 8, 14734.	12.8	184
48	Mechanical Properties of Poly(dopamine) oated Graphene Oxide and Poly(vinyl alcohol) Composite Fibers Coated with Reduced Graphene Oxide and Their Use for Piezoresistive Sensing. Particle and Particle Systems Characterization, 2017, 34, 1600382.	2.3	11
49	Probing Evolution of Twist-Angle-Dependent Interlayer Excitons in MoSe ₂ /WSe ₂ van der Waals Heterostructures. ACS Nano, 2017, 11, 4041-4050.	14.6	227
50	Strain-Mediated Interlayer Coupling Effects on the Excitonic Behaviors in an Epitaxially Grown MoS ₂ /WS ₂ van der Waals Heterobilayer. Nano Letters, 2017, 17, 5634-5640.	9.1	169
51	Thermodynamically Stable Synthesis of Largeâ€Scale and Highly Crystalline Transition Metal Dichalcogenide Monolayers and their Unipolar n–n Heterojunction Devices. Advanced Materials, 2017, 29, 1702206.	21.0	116
52	Imaging of Interlayer Coupling in van der Waals Heterostructures Using a Bright-Field Optical Microscope. Nano Letters, 2017, 17, 5342-5349.	9.1	74
53	Anomalous Ambipolar Transport of Organic Semiconducting Crystals via Control of Molecular Packing Structures. ACS Applied Materials & Interfaces, 2017, 9, 27839-27846.	8.0	10
54	Hydrogenation of monolayer molybdenum diselenide via hydrogen plasma treatment. Journal of Materials Chemistry C, 2017, 5, 11294-11300.	5.5	20

#	Article	IF	CITATIONS
55	Highly stable 3D porous heterostructures with hierarchically-coordinated octahedral transition metals for enhanced performance supercapacitors. Nano Energy, 2017, 39, 337-345.	16.0	72
56	Hexagonal Boron Nitride/Au Substrate for Manipulating Surface Plasmon and Enhancing Capability of Surface-Enhanced Raman Spectroscopy. ACS Nano, 2016, 10, 11156-11162.	14.6	64
57	Wafer-Scale and Wrinkle-Free Epitaxial Growth of Single-Orientated Multilayer Hexagonal Boron Nitride on Sapphire. Nano Letters, 2016, 16, 3360-3366.	9.1	167
58	Chemical Vapor Deposition of Highâ€Quality Large‧ized MoS ₂ Crystals on Silicon Dioxide Substrates. Advanced Science, 2016, 3, 1500033.	11.2	128
59	High-quality graphene via microwave reduction of solution-exfoliated graphene oxide. Science, 2016, 353, 1413-1416.	12.6	670
60	Prevention of Transition Metal Dichalcogenide Photodegradation by Encapsulation with h-BN Layers. ACS Nano, 2016, 10, 8973-8979.	14.6	70
61	A General Approach to Preferential Formation of Active Fe–N _{<i>x</i>} Sites in Fe–N/C Electrocatalysts for Efficient Oxygen Reduction Reaction. Journal of the American Chemical Society, 2016, 138, 15046-15056.	13.7	663
62	Selective synthesis of pure cobalt disulfide on reduced graphene oxide sheets and its high electrocatalytic activity for hydrogen evolution reaction. Nano Convergence, 2016, 3, 5.	12.1	25
63	Support-Free Transfer of Ultrasmooth Graphene Films Facilitated by Self-Assembled Monolayers for Electronic Devices and Patterns. ACS Nano, 2016, 10, 1404-1410.	14.6	69
64	Phase-engineered transition-metal dichalcogenides for energy and electronics. MRS Bulletin, 2015, 40, 585-591.	3.5	71
65	Synthesis and structure of two-dimensional transition-metal dichalcogenides. MRS Bulletin, 2015, 40, 566-576.	3.5	43
66	Multiple Redox Modes in the Reversible Lithiation of High-Capacity, Peierls-Distorted Vanadium Sulfide. Journal of the American Chemical Society, 2015, 137, 8499-8508.	13.7	127
67	Unveiling Surface Redox Charge Storage of Interacting Two-Dimensional Heteronanosheets in Hierarchical Architectures. Nano Letters, 2015, 15, 2269-2277.	9.1	80
68	Catalytic Conversion of Hexagonal Boron Nitride to Graphene for In-Plane Heterostructures. Nano Letters, 2015, 15, 4769-4775.	9.1	52
69	Monolayer-Precision Synthesis of Molybdenum Sulfide Nanoparticles and Their Nanoscale Size Effects in the Hydrogen Evolution Reaction. ACS Nano, 2015, 9, 3728-3739.	14.6	201
70	Atomic-scale dynamics of triangular hole growth in monolayer hexagonal boron nitride under electron irradiation. Nanoscale, 2015, 7, 10600-10605.	5.6	63
71	Seamless Stitching of Graphene Domains on Polished Copper (111) Foil. Advanced Materials, 2015, 27, 1376-1382.	21.0	314
72	VS2/rGO hybrid nanosheets prepared by annealing of VS4/rGO. Journal of Solid State Chemistry, 2015, 224. 82-87.	2.9	46

#	Article	IF	CITATIONS
73	Graphene oxide nanopaint. Carbon, 2014, 72, 328-337.	10.3	163
74	High yield exfoliation of two-dimensional chalcogenides using sodium naphthalenide. Nature Communications, 2014, 5, 2995.	12.8	655
75	Recent advances in layered transition metal dichalcogenides for hydrogen evolution reaction. Journal of Materials Chemistry A, 2014, 2, 5979-5985.	10.3	258
76	Lithium reaction mechanism and high rate capability of VS ₄ –graphene nanocomposite as an anode material for lithium batteries. Journal of Materials Chemistry A, 2014, 2, 10847-10853.	10.3	118
77	Superstructural defects and superlattice domains in stacked graphene. Carbon, 2014, 80, 755-761.	10.3	12
78	Stacking of Two-Dimensional Materials in Lateral and Vertical Directions. Chemistry of Materials, 2014, 26, 4891-4903.	6.7	96
79	Catalyst-Free Synthesis of Si-SiO _{<i>x</i>} Core-Shell Nanowire Anodes for High-Rate and High-Capacity Lithium-Ion Batteries. ACS Applied Materials & Interfaces, 2014, 6, 6340-6345.	8.0	52
80	Poly(vinyl alcohol) Reinforced and Toughened with Poly(dopamine)-Treated Graphene Oxide, and Its Use for Humidity Sensing. ACS Nano, 2014, 8, 6739-6747.	14.6	197
81	Substrate and buffer layer effect on the structural and optical properties of graphene oxide thin films. RSC Advances, 2013, 3, 5926.	3.6	43
82	Mosaic-like Monolayer of Graphene Oxide Sheets Decorated with Tetrabutylammonium Ions. ACS Nano, 2013, 7, 8082-8088.	14.6	30
83	Twoâ€Dimensional Hybrid Nanosheets of Tungsten Disulfide and Reduced Graphene Oxide as Catalysts for Enhanced Hydrogen Evolution. Angewandte Chemie - International Edition, 2013, 52, 13751-13754.	13.8	474
84	Selective formation of thickness-controlled fullerene disks by vapor–solid process. Journal of Crystal Growth, 2013, 363, 141-144.	1.5	4
85	Freeze-dried WS2 composites with low content of graphene as high-rate lithium storage materials. Journal of Materials Chemistry A, 2013, 1, 14548.	10.3	89
86	The chemistry of two-dimensional layered transition metal dichalcogenide nanosheets. Nature Chemistry, 2013, 5, 263-275.	13.6	8,051
87	Enhanced optical response of hybridized VO2/graphene films. Nanoscale, 2013, 5, 2632.	5.6	36
88	Growth of High-Crystalline, Single-Layer Hexagonal Boron Nitride on Recyclable Platinum Foil. Nano Letters, 2013, 13, 1834-1839.	9.1	336
89	Three-dimensional pillared metallomacrocycle–graphene frameworks with tunable micro- and mesoporosity. Journal of Materials Chemistry A, 2013, 1, 8432.	10.3	32
90	Flexible Thermochromic Window Based on Hybridized VO ₂ /Graphene. ACS Nano, 2013, 7, 5769-5776.	14.6	154

#	Article	IF	CITATIONS
91	Synthesis and Characterization of Patronite Form of Vanadium Sulfide on Graphitic Layer. Journal of the American Chemical Society, 2013, 135, 8720-8725.	13.7	300
92	Large-Scale Graphene Micropatterns via Self-Assembly-Mediated Process for Flexible Device Application. Nano Letters, 2012, 12, 743-748.	9.1	68
93	Large-scale patterning by the roll-based evaporation-induced self-assembly. Journal of Materials Chemistry, 2012, 22, 22844.	6.7	18
94	Epoxy to Carbonyl Group Conversion in Graphene Oxide Thin Films: Effect on Structural and Luminescent Characteristics. Journal of Physical Chemistry C, 2012, 116, 19010-19017.	3.1	83
95	Oxidation Resistance of Iron and Copper Foils Coated with Reduced Graphene Oxide Multilayers. ACS Nano, 2012, 6, 7763-7769.	14.6	175
96	Reversibly Light-Modulated Dirac Point of Graphene Functionalized with Spiropyran. ACS Nano, 2012, 6, 9207-9213.	14.6	85
97	Highly Efficient Polymer Light-Emitting Diodes Using Graphene Oxide as a Hole Transport Layer. ACS Nano, 2012, 6, 2984-2991.	14.6	127
98	Facile Method for rGO Field Effect Transistor: Selective Adsorption of rGO on SAMâ€Treated Gold Electrode by Electrostatic Attraction. Advanced Materials, 2012, 24, 2299-2303.	21.0	26
99	Functionalized graphene sheets/polycarbonate nanocomposites compatibilized by poly(phenylenevinylene). Macromolecular Research, 2012, 20, 768-771.	2.4	3
100	Interaction between Metal and Graphene: Dependence on the Layer Number of Graphene. ACS Nano, 2011, 5, 608-612.	14.6	324
101	Highly controllable transparent and conducting thin films using layer-by-layer assembly of oppositely charged reduced graphene oxides. Journal of Materials Chemistry, 2011, 21, 3438-3442.	6.7	194
102	Large-Area Graphene Films by Simple Solution Casting of Edge-Selectively Functionalized Graphite. ACS Nano, 2011, 5, 4974-4980.	14.6	98
103	Reduced Graphene Oxide (rGO)-Wrapped Fullerene (C ₆₀) Wires. ACS Nano, 2011, 5, 8365-8371.	14.6	63
104	Surfaceâ€Enhanced Raman Scattering of Single―and Few‣ayer Graphene by the Deposition of Gold Nanoparticles. Chemistry - A European Journal, 2011, 17, 2381-2387.	3.3	133
105	Spatially Resolved Spontaneous Reactivity of Diazonium Salt on Edge and Basal Plane of Graphene without Surfactant and Its Doping Effect. Langmuir, 2010, 26, 12278-12284.	3.5	92
106	Transparent, Flexible Conducting Hybrid Multilayer Thin Films of Multiwalled Carbon Nanotubes with Graphene Nanosheets. ACS Nano, 2010, 4, 3861-3868.	14.6	313
107	Effects of nanofluids containing graphene/graphene-oxide nanosheets on critical heat flux. Applied Physics Letters, 2010, 97, .	3.3	162
108	Spontaneous electron transfer from C60 to Au ions: oxidation of C60 and hole doping. Journal of Materials Chemistry, 2010, 20, 7183.	6.7	12

#	Article	IF	CITATIONS
109	Density control of ZnO nanowires grown using Au-PMMA nanoparticles and their growth behavior. Nanotechnology, 2009, 20, 085601.	2.6	16
110	Highly Selective Synthesis of C ₆₀ Disks on Graphite Substrate by a Vapor–Solid Process. Angewandte Chemie - International Edition, 2008, 47, 693-696.	13.8	88
111	Lithium Ions Intercalated into Pyrene-Functionalized Carbon Nanotubes and Their Mass Transport:Â A Chemical Route to Carbon Nanotube Schottky Diode. Journal of the American Chemical Society, 2008, 130, 2160-2161.	13.7	17
112	Two-Dimensional Gradient Mapping Technique Useful for Detailed Spectral Analysis of Polymer Transition Temperatures. Journal of Physical Chemistry B, 2008, 112, 3611-3616.	2.6	16
113	"Fingertip―Guided Noncovalent Functionalization of Carbon Nanotubes by Dendrons. Langmuir, 2007, 23, 11373-11376.	3.5	17
114	Transition temperatures and molecular structures of poly(methyl methacrylate) thin films by principal component analysis: comparison of isotactic and syndiotactic poly(methyl methacrylate). Vibrational Spectroscopy, 2005, 37, 69-76.	2.2	16
115	Spontaneous Formation of Transition-Metal Nanoparticles on Single-Walled Carbon Nanotubes Anchored with Conjugated Molecules. Small, 2005, 1, 975-979.	10.0	54
116	Mechanism of growth of colloidal silver nanoparticles stabilized by polyvinyl pyrrolidone in γ-irradiated silver nitrate solution. Journal of Colloid and Interface Science, 2004, 274, 89-94.	9.4	231
117	Chemical and size effects of nanocomposites of silver and polyvinyl pyrrolidone determined by X-ray photoemission spectroscopy. Chemical Physics Letters, 2004, 383, 418-422.	2.6	94
118	Hydrogen-Bonding Networks of Dialkyl Disulfides Containing the Urea Moiety in Self-Assembled Monolayers. Langmuir, 2004, 20, 1674-1679.	3.5	15
119	Effects of Surface Anchoring Groups (Carboxylate vs Phosphonate) in Ruthenium-Complex-Sensitized TiO2 on Visible Light Reactivity in Aqueous Suspensions. Journal of Physical Chemistry B, 2004, 108, 14093-14101.	2.6	281
120	New Approach to Generalized Two-Dimensional Correlation Spectroscopy. 1: Combination of Principal Component Analysis and Two-Dimensional Correlation Spectroscopy. Applied Spectroscopy, 2002, 56, 1562-1567.	2.2	65
121	Characterization of Transition Temperatures of a Langmuir—Blodgett Film of Poly(tert-butyl) Tj ETQq1 1 0.7843 Applied Spectroscopy, 2002, 56, 1568-1574.	14 rgBT /C 2.2	Overlock 10 42
122	Glass Transition Temperature and Conformational Changes of Poly(methyl methacrylate) Thin Films Determined by a Two-Dimensional Map Representation of Temperature-Dependent Reflectionâ´'Absorption FTIR Spectra. Langmuir, 2002, 18, 5953-5958.	3.5	52
123	Structural Comparison of Langmuirâ^Blodgett and Spin-Coated Films of Poly(tert-butyl methacrylate) by External Reflection FTIR Spectroscopy and Two-Dimensional Correlation Analysis. Langmuir, 2002, 18, 5523-5528.	3.5	26
124	Direct patterning of silver colloids by microcontact printing: possibility as SERS substrate array. Vibrational Spectroscopy, 2002, 29, 79-82.	2.2	23
125	Phase- and composition-controlled synthesis. Nature Materials, 0, , .	27.5	1